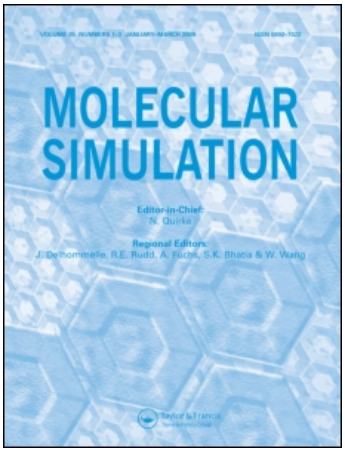

Molecular Simulation
Publication details, including instructions for authors and subscription information:
http://www.informaworld.com/smpp/title~content=t713644482

Monte Carlo Simulations of Adsorption of Non-polar and Polar Molecules in Zeolite *X*

Fokion Karavias[a]; Alan L. Myers[a]
[a] Department of Chemical Engineering, University of Pennsylvania, Philadelphia, PA, USA

To cite this Article Karavias, Fokion and Myers, Alan L.(1991) 'Monte Carlo Simulations of Adsorption of Non-polar and Polar Molecules in Zeolite *X*', Molecular Simulation, 8: 1, 23 — 50
To link to this Article: DOI: 10.1080/08927029108022466
URL: http://dx.doi.org/10.1080/08927029108022466

Molecular Simulation, 1991, Vol. 8, pp. 23–50
Reprints available directly from the publisher
Photocopying permitted by license only

MONTE CARLO SIMULATIONS OF ADSORPTION OF NON-POLAR AND POLAR MOLECULES IN ZEOLITE *X*

FOKION KARAVIAS and ALAN L. MYERS

Department of Chemical Engineering, University of Pennsylvania, Philadelphia, PA 19104, USA

(*Received November, 1990; accepted March 1991*)

Grand canonical Monte Carlo simulations have been performed for single-gas adsorption of Lennard-Jones molecules with point multipole moments in zeolite cavities of type *X*. Fluid-solid electrostatic interactions are taken into account. Adsorption isotherms, isosteric heats and structural properties have been calculated for Xe, CH_4, CO_2, C_2H_4, and i-C_4H_{10} and compared with experiment. The results reveal the importance of adsorbate–adsorbate interactions for sorption in faujasite. The interaction of the quadrupole moment of CO_2 with the electric field generated by the zeolite ions constitutes more than half of the total energy of adsorption. Density and energy distributions show that the cavity is either a relatively homogeneous surface or a highly heterogeneous one, depending on the molecular characteristics of the adsorbed gas and the type, position and charge of the zeolite cations.

KEY WORDS: Zeolites, adsorption, Monte Carlo simulation.

INTRODUCTION

Zeolites or molecular sieves are microporous crystalline aluminosilicates used commercially in a wide range of applications such as chromatography, ion exchange, catalysis and separation technology.

Despite the widespread use of zeolites as adsorbents, there is no satisfactory equation for calculating the adsorption of molecules and their mixtures. Thermodynamic models for the prediction of multicomponent adsorption equilibria from single-component isotherm data either rely on the assumption of an ideal adsorbed solution or use activity coefficients derived from experimental binary data.

Computer simulations, which have been widely used to model bulk-liquid interfaces and molecules adsorbed on flat surfaces, provide an excellent tool for studying the behavior of adsorbed molecules in zeolites.

SURVEY OF PREVIOUS WORK

Studies of single-gas adsorption in zeolites by Monte Carlo (MC) or Molecular Dynamics (MD) already exist in the literature. Stroud and coworkers [1] applied the Lennard-Jones Devonshire [2] cell theory of fluids to obtain a spherically-averaged potential model without electrostatic forces for zeolite cavities of type 5A. Monte Carlo simulations of the canonical ensemble gave fairly good agreement with experimental data for methane adsorption isotherms and isosteric heats, but not for heat capacities.

Soto and Myers [3] extended this model by adding the contribution of induced electrostatic forces and performed grand canonical MC simulations of Kr in a zeolite MS-13*X* cavity at 183 K. Bezus, Kiselev *et al.* [4–6] calculated Henry's constants and isosteric heats of adsorption at zero coverage for non-polar and polar inorganic molecules and hydrocarbons adsorbed in zeolites of type *X* and *Y*. The atom–atom approximation was used to calculate the potential energy of the intermolecular interaction of non-polar molecules. For polar molecules, an allowance was also made for the electrostatic interaction of the rigid molecular multipoles with zeolite ions. The contribution was calculated using the point moment approximation.

More recently, June and coworkers [7] developed a model of ZSM-5 zeolite using the atom–atom approximation and evaluated Henry's constants and isosteric heats of sorption of hydrocarbons by MC integration, and diffusion coefficients by MD simulation. To reduce computer time, they calculated the total gas–solid energy and fitted the energy function with a three-dimensional cubic spline. Woods and Rowlinson [8,9] presented grand canonical MC simulations of Xe and CH_4 in zeolites of type *X* and *Y* (faujasite). They used two models: a simple one based on a spherically-averaged potential for a single isolated cavity and a detailed one based on the atom–atom approximation for eight large cavities. Interactions between adsorbate molecules and the ions of the zeolite framework were modeled in terms of short range potentials; no long-range forces were taken into account. An interesting result of this work is that the adsorption isotherms for Xe calculated by the two different models agree very well at low and medium occupancies.

Razmus and Hall [10] presented grand canonical MC simulations of N_2, O_2 and their binary mixture in zeolite 5A. They used a point multipole model for both molecules and calculated single-gas isotherms, isosteric heats and selectivities for the binary mixture. The atom-atom approximation, with interactions of both short-range Lennard–Jones and long-range coulombic forces, was used by Yashonath and coworkers [11,12] in their molecular simulation of CH_4 in eight supercages of zeolite Na*Y*. They performed MC simulation of the canonical ensemble and MD in the microcanonical ensemble. Energy and spatial distributions, diffusion coefficients and residence time of an adsorbate molecule in a supercage were calculated.

Although detailed models based on the atom–ion approximation were very successful in predicting isotherms and isosteric heats, they were also expensive, requiring hours of supercomputer time. The aim of this paper is to show that an improved spherically-averaged potential for the dispersion–repulsion term, coupled with the contribution of the interaction of the electrostatic field with the molecular multipoles, gives an accurate representation of adsorption in faujasite in a fraction of the time required by other models. Since no simulations of polar molecules in Na*X* have been reported, further investigation of the polar nature of this zeolite is justified. The objective of this work is to test the ability of computer simulations to predict adsorption in zeolites. Furthermore, the simulations serve as a model system for testing thermodynamic or statistical mechanical theories for single-gas adsorption.

Simulations of Xe, CH_4, CO_2, C_2H_4, and i-C_4H_{10} in zeolite 13*X* have been performed. These molecules can be simulated as Lennard–Jones molecules with point multipole moments. Moreover, experimental single-gas isotherms are available.

CAVITY MODEL AND POTENTIALS

The building block of faujasite is the truncated octahedron or sodalite unit containing

24 (Si^{+4}, Al^{+3}) ions interconnected with 36 oxygens. The sodalite units, called β cages, are inaccessible to the adsorbate molecules but they are joined together to form large cavities or supercages with a radius of about 7 Å. A particularly important feature of faujasite is that the large cavities are interconnected in a tetrahedral arrangement through almost circular windows of diameter 7.5 Å to give a highly porous material. Each supercage has four nearest-neighbor cavities at a distance of 10.81 Å and twelve second nearest-neighbor cavities at 17.6 Å. The framework of the molecular sieves is completed by several cations (Ca^{++}, Na^{+}) which serve to neutralize the overall charge of the zeolite crystal. The cations are mainly responsible for the energetic heterogeneity of the molecular sieves; their charge and position affect properties of the adsorbent such as adsorptive capacity and selectivity.

The ions forming the walls of the large cavities lie roughly in a spherical shell and therefore zeolites may be considered to be a collection of identical, nearly spherical cavities, Figure 1.

The state-of-the-art in calculating the gas–solid potential energies is to assume pairwise-additive potentials and sum over the ions of the zeolite crystal (atom–ion approximation). Although this method is sound, it requires several hours of super-computer time.

In this work, we take advantage of the nearly spherical shape of the zeolite cavities. A spherically-averaged potential for the dispersion and repulsion term is adopted. The main assumption is that all surface ions are located at the same distance from the center of the cavity and that the dispersion and repulsion interaction terms between the fluid molecule and each ion of the cavity may be modelled by a Lennard–Jones potential. Then the Lennard–Jones Devonshire theory [2], which was first developed for liquids, can be applied to calculate the dispersion and repulsion (short-range term)

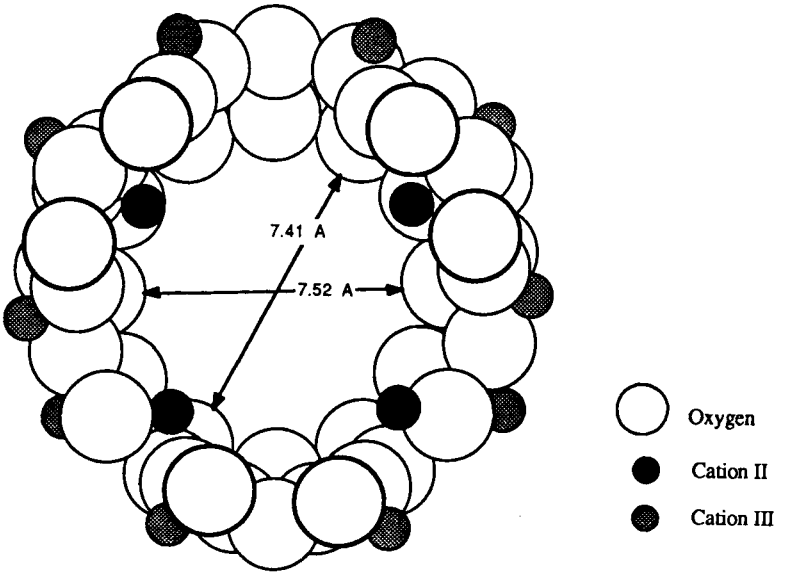

Figure 1 Cross-section of 13*X* adsorption cavity.

cavity potential [1,13]:

$$\Psi_{is}^{dr}(r) = 4C\,\varepsilon_{is}\left[\left(\frac{\sigma_{is}}{R}\right)^{12} L\left\{\frac{r^2}{R^2}\right\} - \left(\frac{\sigma_{is}}{R}\right)^{6} M\left\{\frac{r^2}{R^2}\right\}\right] \tag{1}$$

$$L\{x\} = (1 + 12x + 25.2x^2 + 12x^3 + x^4)/(1 - x)^{10}$$

where

$$M\{x\} = (1 + x)/(1 - x)^4$$

$\Psi_{is}^{dr}(r)$ is a function of r, the radial distance of the adsorbed molecule from the center of the cavity. The cavity radius R is chosen as the distance from the center to the nearest oxygen atom. For a $13X$ zeolite cavity $R = 7.057$ Å [13,14]. ($C\,\varepsilon_{is}$) and σ_{is} are the Lennard-Jones energy and collision parameters of molecule i with the solid wall.

The ions in the zeolite crystal create an electrostatic field **E(r)** inside the cavity, which induces electrostatic forces that act upon the adsorbed molecules. The induction electrostatic potential is non-pairwise additive and has the form [15]:

$$\Psi_i^{ind} = -\left[\frac{\alpha_i}{2} + \frac{1}{3}(\alpha_{\|i} - \alpha_{\perp i})(3\cos^2\theta + 1)\right]\mathbf{E(r)}^2 \tag{2}$$

where $\alpha_i = \frac{1}{3}(\alpha_{\|i} + 2\alpha_{\perp i})$ is the average polarizability, $\alpha_{\|i}$ is the polarizability along the internuclear axis and $\alpha_{\perp i}$ is perpendicular to the internuclear axis. The electrostatic field **E(r)** is generated by the ions in the zeolite crystal. If we had to consider the contributions of both the oxygen ions and cations (the oxygen ions are 8 to 10 times more plentiful than the cations), the many-body induction term would increase the computational time significantly. Fortunately, the contribution of the cations dominates [5]. The oxygen ions are almost uniformly and symmetrically distributed around the cavity surface, Figure 1; therefore the electric field they produce inside the cavity is weak. Razmus and Hall [10], who studied adsorption in zeolite 5A, assumed a negative charge of $-\frac{1}{3}$ for the oxygen ions adjacent to the cations and a neutral charge for the rest of the oxygens. In the proposed model the contribution of the oxygen ions is omitted and an effective charge of $z_l = +0.58$ is assigned to the cations closest to the cavity wall. This value was extracted by fitting Xe second virial coefficients of adsorption to experimental data and was used in the simulations of all the compounds studied in this work. There are 14 cations in a $13X$ cavity [13,14] and their coordinates are presented in Table 1. Since the ions in the zeolite cavities have some degree of the mobility [16], the four Na^+ ions of type II were moved from 5.78 Å to 6.80 Å from the center of the cavity. Following Soto *et al.* [13], this adjustment for ion locations was made to compensate for the actual repulsive forces which surround

Table 1 Position and effective charge of cations for the $13X$ zeolite cavity.

			Coordinates, Å			
Cation	*No. of sites*	z_l	x	y	z	r
Sodium (II)	4[a]	+ 0.580	3.930	3.930	3.930	6.807
Sodium (III)	10[b]	+ 0.580	− 1.245	6.227	6.227	8.894

[a] 4 ions are placed at (x, y, z), $(x, -y, -z)$, $(-x, y, -z)$ and $(-x, -y, z)$

[b] 10 ions are placed at $(x, -y, -z)$, $(-x, -y, z)$, $(-x, y, -z)$, (z, x, y), $(z, -x, -y)$, (z, y, x), $(z, -y, -x)$, $(-z, y, -x)$, $(-z, -y, x)$ and $(-z, -x, y)$

these ions when adsorbate molecules overlap their electron clouds. The electric field inside the cavity is calculated as:

$$E^2 = E_x^2 + E_y^2 + E_z^2 \tag{3}$$

where

$$E_q = \sum_l z_l \frac{q_l - q_i}{r^3} \quad \{q = x, y, z\}$$

and z_l is the effective charge of the lth cation, q_l is the coordinate of the cation, q_i the coordinate of molecule of component i and r the distance between the cation and the molecule. In Equation (2) the second term on the right-hand-side is proportional to the difference $(\alpha_{\|i} - \alpha_{\perp i})$. Although other workers have neglected this term, it is significant for linear molecules like CO_2 and is included in our calculations.

Electrostatic interactions of adsorbate molecules with the electric field generated by the ions are modeled as point multipole moments. The potential of a molecule with a point quadrupole moment Q_i interacting with the cavity ions is [15]:

$$\Psi_i^Q = \frac{1}{2} \sum_l z_l Q_i \frac{3 \cos^2\theta - 1}{r^3} \tag{4}$$

where Q_i is the quadrupole moment of the adsorbate, z_l is the effective charge of the cations, and θ is the angle between the line joining the center of the molecule with the cation and the vector determining the orientation of the adsorbate. The summation is over all the cations of the cavity that are included in the model.

Thus the total potential energy of interaction of the molecules with the wall is:

$$\Psi = \Psi^{dr} + \Psi^{ind} + \Psi^{Q} \tag{5}$$

The 'sphericalization process', although reasonable for short-range forces, would cause the electric field to vanish inside the cavity if it were applied to the electric charge of the ions. The interaction energy of an adsorbed molecule with the electrostatic field inside the cavity has to be calculated by a direct summation over the nearest cations.

For a single adsorbed gas, the total potential has two adjustable parameters, $(C\varepsilon_{is})$ and σ_{is}, which are obtained by fitting adsorption second virial coefficients versus temperature to experimental data. Second virial coefficients were calculated at different temperatures by Monte Carlo integration:

$$B_{is} = \int \exp(-\beta\Psi)\, d\mathbf{r}\, d\Omega \tag{6}$$

where B_{is} is the second virial coefficient, $\mathbf{r}$ designates the coordinates of the center of the molecule and Ω represents the Euler's angles by which the orientation of the molecule (CO_2, C_2H_4) is specified. The experimental values of B_{is} were extracted from the data discussed in the results section by fitting experimental measurements to empirical isotherms (Unilan and Toth Equations [17]).

Dispersion and repulsion adsorbate-adsorbate interactions are modelled by the Lennard-Jones 12-6 potential:

$$U_{ij}^{dr}(r) = 4\varepsilon_{ij}\left[\left(\frac{\sigma_{ij}}{r}\right)^{12} - \left(\frac{\sigma_{ij}}{r}\right)^{6}\right] \tag{7}$$

where ε_{ij} and σ_{ij} are the LJ energy and collision parameters respectively, and r is the distance between two adsorbed molecules.

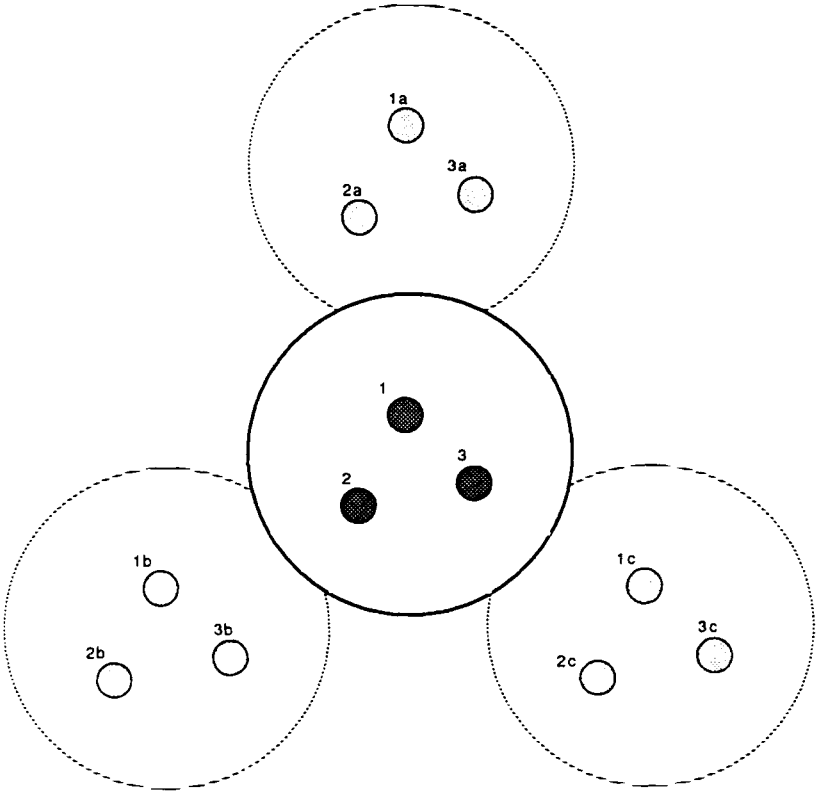

Figure 2 Top view of a central zeolite cavity interacting with three of its four nearest-neighbors. Each nearest-neighbor cavity is a periodic image of the central one. Molecule 1 interacts with molecules 2 and 3 and their periodic images, $1i$, $2i$, $3i$ $\{i = a, b, c, d\}$.

Previous workers who used the spherical cavity model assumed that the supercages in the zeolite crystal are independent, so that lateral interactions between molecules adsorbed in different cavities could be ignored. However, in zeolites of type A and for faujasite, the large cavities are closely connected and the potential between molecules of nearest-neighbor supercages makes a large contribution to adsorbate–adsorbate energies. It is assumed that the nearest-neighbor cavities are periodic images of the central cavity; therefore they have the same number of molecules located at the same relative positions. Figure 2 shows a top view of the tetrahedral arrangement of the cavities. The interactions between a molecule in the central cavity and all of its periodic images are taken into account. The Lennard-Jones potential between a molecule lying in the central cavity and a periodic image molecule is:

$$U_{ij}^{dr}(\mathbf{r} + \mathbf{n}) = 4\varepsilon_{ij}\left[\left(\frac{\sigma_{ij}}{|\mathbf{r} + \mathbf{n}|}\right)^{12} - \left(\frac{\sigma_{ij}}{|\mathbf{r} + \mathbf{n}|}\right)^{6}\right] \tag{8}$$

where $\mathbf{n} = (n_x, n_y, n_z)L$, with n_x, n_y, n_z integers and $|\mathbf{n}|$ is the nearest-neighbor intercavity distance. The prime indicates that the potential refers to nearest-neighbor cavity interactions. In faujasite X, $L = 6.24$ Å [14] and there are four nearest-neigh-

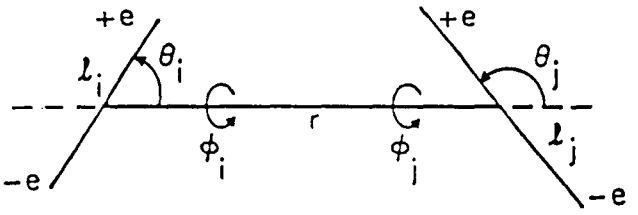

Figure 3 Relative orientation of two linear molecules.

bor supercages in a tetrahedral arrangement (1,1,−1), (1,−1,1), (−1,1,1), (−1,−1,−1). Although no cut-off distance was used for the fluid–fluid potential, the interaction of a molecule of the central cavity with those of the nearest-neighbor cavities implies a cut-off distance equal to the intercavity distance, which is 10.81 Å for faujasite.

Lateral interactions between multipolar molecules should also be taken into account. If the molecules have quadrupole moments Q then the potential is [18]:

$$U_{ij}^{QQ} = \frac{3}{4}\frac{Q_i Q_j}{r^5}(1 - 5c_1^2 - 5c_2^2 + 17c_1^2c_2^2 + 2s_1^2s_2^2c_{12}^2 - 16s_1s_2c_1c_2c_{12}) \tag{9}$$

where $s_i = \sin\theta_i$, $c_i = \cos\theta_i$ and $c_{12} = \cos(\phi_1 - \phi_2)$. The angles θ_i and ϕ_i depend on the relative orientation of the two linear dipoles, Figure 3. Therefore, the total lateral interaction potential is:

$$U = U^{dr} + U^{QQ} \tag{10}$$

Polar molecules in the central cavity are allowed to interact with those of nearest-neighbor cavities.

The proposed model is not the most rigorous of the literature for single component adsorption. Other researchers have presented more exact models (e.g. atom-atom summation). Although our model is less exact, it can be implemented on a workstation without sacrificing accuracy. Dispersion–repulsion and electrostatic potentials between the solid and the fluid, adsorbate–adsorbate interactions, and the effect of nearest-neighbor cavities are taken into account. In our model:

a) The effect of the windows of which interconnect the supercages is not included.
b) Migration of molecules between cavities is not allowed.

Table 2 Potential parameters for gases adsorbed in zeolite 13X

Molecule	$C\varepsilon_{is}/k^{(a)}$ K	$\sigma_{is}^{(a)}$ Å	ε_{ii}/k K	σ_{ii} Å	α_i $10^{-24}cm^3$	$(\alpha_{\parallel i} - \alpha_{\perp i})$ $10^{-24}cm^3$	Q_i 10^{-26} e.s.u. cm^2
Xe	15,500	3.38	231.0 [24]	4.047 [24]	4.01 [38]	0.00	0.00
CH_4	12,000	3.375	148.6 [36]	3.82 [36]	2.60 [38]	0.00	0.00
CO_2	15,500	3.375	225.0 [37]	3.80 [37]	2.65 [38]	2.04 [38]	− 4.30 [39]
C_2H_4	15,550	3.430	224.7 [24]	4.163 [24]	4.26 [38]	1.35 [38]	− 3.92 [39]
i-C_4H_{10}	18,800	3.930	330.1 [24]	5.278 [24]	8.32(*b*)	0.00	0.00

*a*Values obtained from experimental data for adsorption 2nd virial coefficients.
*b*Value was obtained by Silberstein method [28].

c) Adsorbed molecules are structureless and the effect of rotational degrees of freedom is omitted.

As will be shown, our simulation results are close to those of more expensive models and to experimental measurements. The potential parameters of all components are presented in Table 2.

THE SIMULATION METHOD

A series of GCMC simulations of single-gas adsorption were performed for adsorption. The simulations follow the methods developed for bulk fluids [19,20] and fluids adsorbed in cylindrical pores and slits [21]. The procedure is given below (see also Figure 4):

Initial Configuration and Equilibration

Depending on the value of the chemical potential, 2–12 molecules are placed at random locations inside the zeolite cavity at the start of a run. An insertion is accepted only if the total energy of the system is less than zero. Because the simulation starts from a random configuration, the first 10,000–50,000 cycles are discarded. Each simulation is divided into ten blocks and it is assumed that the system has reached equilibrium if the results of the first block are within the standard deviation of the results from the following blocks.

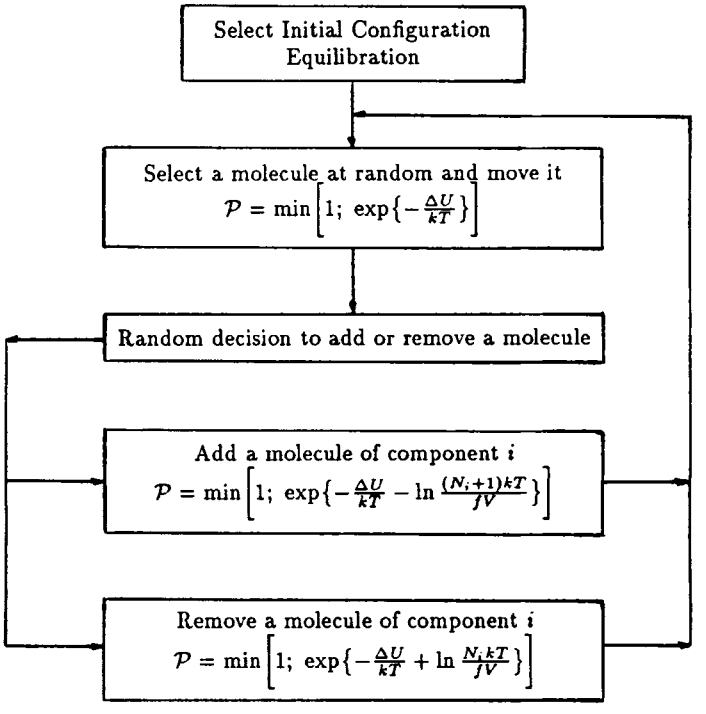

Figure 4 Algorithm for Monte Carlo simulation of a grand canonical ensemble.

Displacement Steps

Displacements are handled using the normal Metropolis method. The maximum allowed displacement is adjusted during the simulation to give an average acceptance ratio of 50% for the attempted moves. In the case of linear molecules a new orientation must also be selected. Two additional random numbers from a uniform distribution are chosen to represent $\cos\theta$ and ϕ, normalized to the range -1 to 1 and 0 to 2π. Each displacement move is followed by two creation or destruction steps. Thus, moves, destructions and creations are selected at random with equal probability to optimize the convergence to the Markov chain [19].

Creation and Destruction Steps

A random decision is made whether to try to add a molecule to the cavity or try to remove one.

In the creation step, a position in the cavity is chosen at random and a new configuration is created by inserting a molecule at this position. If the molecule is linear its orientation is also chosen randomly. The particle creation is accepted with probability:

$$\mathscr{P} = \min\left[1; \exp\left\{-\frac{\Delta U}{kT} - \ln\frac{(N_i + 1)kT}{fV}\right\}\right] \tag{11}$$

where ΔU is the configurational energy change for creation of a particle, N_i is the current number of molecules of component i in the cavity before the attempted creation, $V(=\frac{4}{3}\pi R^3)$ is the volume of the cavity and f is the fugacity in the gas phase.

In the destruction step, a molecule is chosen at random and a new configuration is created by removing the molecule from the cavity. The particle destruction is accepted with probability:

$$\mathscr{P} = \min\left[1; \exp\left\{-\frac{\Delta U}{kT} + \ln\frac{N_i kT}{fV}\right\}\right] \tag{12}$$

Convergence problems may arise in a GCMC simulation, particularly for fluctuation quantities, when the system density is near that of a dense fluid [22]. These problems arise from low acceptance ratios for creation attempts. Adams [20] argued that ensemble averages are not affected and Mezei [23] showed that liquid densities calculated by GCMC are quite accurate even when the acceptance ratio for particle creation steps is as low as 0.1%. In systems like ours where the density is inhomogeneous, holes large enough to accomodate a new particle can be found and the acceptance ratio exceeds 0.1%.

The total number of cycles (one cycle included the move and creation–destruction steps) necessary to achieve an acceptable accuracy depends on the density, the molecule simulated and the number of components. In the case of xenon, methane and isobutane, 2×10^6 cycles were run for each value of the chemical potential, which required 0.5–1.3 h of CPU time on a workstation running at about 2 MFLOPS. For carbon dioxide and ethylene, 3×10^6 cycles or 2–10 h of CPU time were needed because of the calculation of molecular orientation at each step. Since the simulation box was the interior of the zeolite cavity, no more than 13 molecules were present in each configuration and a long Markov chain was needed for good statistics. Our computer time was small compared to 1–3 h on a Cray XMP reported by Woods and

Rowlinson [9] for the Xe–CH_4 system and potentials based on the atom–ion approximation. Our simulations of CO_2 and C_2H_4 were relatively expensive due to the quadrupole interactions involving trigonometric functions.

Temperature, chemical potential, and volume are the independent variables in the grand canonical ensemble. The chemical potential was related to the gas-phase pressure by the Lee-Kesler equation of state [24], given the critical properties of Xe, CH_4, CO_2, C_2H_4, i-C_4H_{10}. The Lee-Kesler equation is solved numerically for the energy and pressure of the gas as a function of the chemical potential and temperature.

Important quantities for adsorption systems are the isosteric (q_{st}) and the differential (q_d) heat. Isosteric heat is defined as the difference of the partial molar enthalpies of the adsorbed and the bulk phase [25]:

$$q_{st} = H^b - H^a = \left(\frac{\partial U^b}{\partial N^b}\right)_T - \left(\frac{\partial U^a}{\partial N^a}\right)_T + pV^b - pV^a \tag{13}$$

where all the properties refer to their configurational part and the superscripts a, b stand for the adsorbed and bulk phase respectively. Since $V^a \ll V^b$, the isosteric heat can be calculated as:

$$q_{st} = -(H^{b,id} - H^b) + kT - \left(\frac{\partial U^a}{\partial N^a}\right)_T \tag{14}$$

where the quantity $(H^{b,id} - H^b)$ is the departure function of the bulk fluid enthalpy calculated by the Lee-Kesler equation of state and $q_d = -(\partial U^a/\partial N^a)_T$ is the differential heat of adsorption. The differential heat can be calculated either by a numerical differentiation of the simulation results for energy or by ensemble fluctuations [25]:

$$q_d = -\frac{f(U,N)}{f(N,N)} \tag{15}$$

where the notation $f(X,Y) = \langle XY\rangle - \langle X\rangle\langle Y\rangle$ stands for the fluctuation of any X-Y pair. The integral of the differential heat obtained by the ensemble fluctuation method is calculated numerically:

$$U(N) = \int\left(\frac{\partial U^a}{\partial N^a}\right)_T dN = \int\frac{f(U,N)}{f(N,N)}dN \tag{16}$$

The ensemble fluctuation method is checked by comparing the energy calculated from equation (16) with the average energy of the simulation. The agreement was within 2% for these simulations.

RESULTS AND DISCUSSION

The effect of Fluid–Fluid Interactions in Zeolite X: Adsorption of Xenon

Simulations of xenon in zeolite 13X were performed. Three isotherms of Xe adsorbed in zeolite 13X at 213.5 K are compared with experimental measurements of Aristov *et al.* [26] in Figure 5. From X-ray crystallographic data [14], there are 3.60×10^{23} cavities per kg of anhydrous NaX; this value is used to convert experimental data to units of number of molecules per cavity. Curve (1) corresponds to Xe hard-sphere GCMC results. Adsorbate–absorbent interactions were modeled by equations (1) and

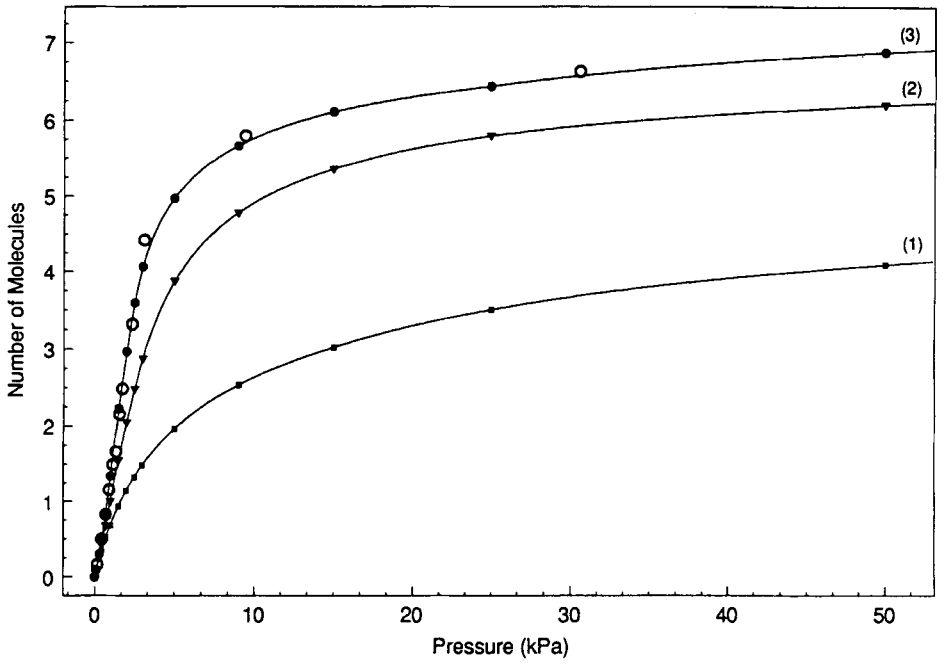

Figure 5 Average occupancy as a function of pressure for Xe at 213.15 K in a 13*X* cavity. (●) MC results with the effect of nearest-neighbor cavities. (▼) MC results when nearest-neighbor cavities are neglected. (■) MC results for hard-spheres. (○) Experimental measurements of Aristov *et al.* for zeolite Na*X* at 213.15 K.

(2). However, fluid–fluid dispersion interactions were not taken into account, and a hard-sphere potential was adopted:

$$U_{ij} = \begin{cases} \infty, & \text{if } r_{ij} < \sigma_{ij} \\ 0, & \text{if } r_{ij} \geqslant \sigma_{ij} \end{cases} \tag{17}$$

where σ_{ij} was taken as the collision diameter of Lennard–Jones potential in Table 2. The predicted coverage is considerably lower than the experimental measurements. Curve (2) in Figure 5 corresponds to Xe simulation results in which the effect of nearest-neighbor cavities is neglected. Adsorbate-adsorbent interactions are modelled by equations (1) and (2), and the fluid–fluid potential is Equation (7). However, if the central-cavity molecules do not interact with those in nearest-neighbor cavities, the calculated average occupancies show systematic deviation from the experimental data. When the interactions of molecules adsorbed in nearest-neighbor cavities are included in the model by Equation (8), the GCMC predictions are in close agreement with the experimental data as shown by curve (3). A comparison of the three curves of Figure 5 reveals the importance of adsorbate–adsorbate interactions for sorption in molecular sieves.

Fluid–fluid and fluid–solid contributions to the configurational part of the internal energy are given in Table 3. Of course fluid–fluid interactions depend upon cavity filling and vanish at the limit of zero pressure. Other computers simulations of Xe in faujasite have neglected the induced electrostatic term by absorbing it into the

Table 3 Percentage contribution of dispersion and electrostatic terms to total energy of adsorption at high coverage in 13*X* zeolite.

		FLUID-SOLID			
Molecule	$\langle N \rangle$	*Disp.*	*Ion-Quad.*	*Ind. Elect.*	*FLUID-FLUID*
Xe	6.5	75	0	6	19
CH_4	7.0	81	0	5	14
$i\text{-}C_4H_{10}$	3.9	82	0	9	9
CO_2	9.0	40	35	9	16
C_2H_4	6.2	48	32	10	10

dispersion term. Woods and Rowlinson [9], for instance, increased the dispersion contribution by 12% to compensate for their neglect of the induced electrostatic term.

Figure 6 presents the MC results for the isosteric heat of Xe molecules at 213 K from Equations (14)–(15). Internal consistency of the simulations was tested by comparing the integral of the differential heat obtained by the fluctuation method with the total energies, which are ensemble averages. The agreement was within 2%. The isosteric heat of Xe in zeolite 13*X* increases linearly with coverage at low and medium occupancies. It attains a constant value at a coverage of 6–8 molecules per cavity and then drops as the coverage approaches saturation. The initial increase in the isosteric heat results from the cooperative effect of adsorbate-adsorbate interactions. The drop at high occupancies is due to the contribution of the bulk-fluid term at high pressures, Equation (14).

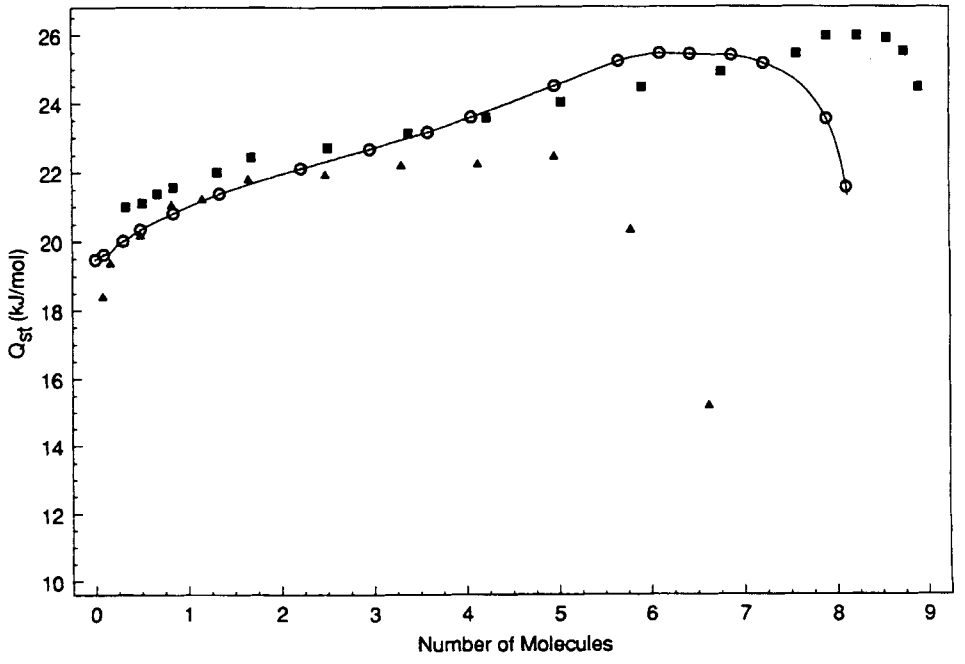

Figure 6 Isosteric heat as a function of coverage for Xe in zeolite 13*X*. (○) MC results at 213.15 K. (▲) Experimental measurements of Aristov *et al.* at 210.9 K. (■) Experimental measurements of Fomkin *et al.* at 150 K.

The predicted values of isosteric heat are compared with two sets of experimental measurements, the data at Aristov *et al.* [26] at 213 K and the data of Fomkin *et al.* [27] at 150 K. The simulation results agree quantitatively with experiment at low occupancies and qualitatively at high coverage. Since the isosteric heat is quite sensitive to the assumptions of the model, the agreement of the GCMC results with the experimental data should be considered very good.

Woods and Rowlinson [9] have also performed simulations of Xe in zeolite *X* by using a more detailed model (atom–ion approximation). Since our simulations agree very well with their results, the simplified spherically-averaged model reduces the computer time without much loss of accuracy.

Adsorption of Lennard–Jones Moelcules: Methane and Isobutane

Methane is a spherically symmetrical molecule without dipole or quadrupole moments and a relatively small polarizability. Lennard–Jones potential parameters are given in Table 2. Isobutane is an almost spherical molecule with a small permanent dipole moment (0.1 D) and a large polarizability. Since the dipole contributes less than 1% of the total energy of adsorption, it has been neglected in our model. The molecular polarizability of isobutane was estimated by the Silberstein method [28], since no experimental measurements were available. The method is based on the

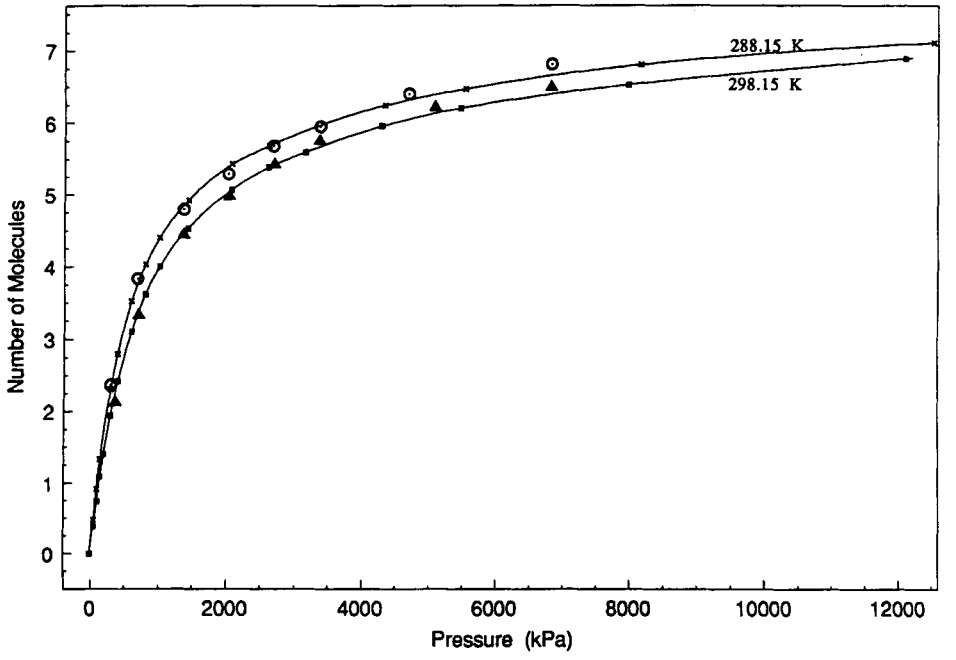

Figure 7 Average occupancy as a function of pressure for CH_4 in a 13*X* cavity. (×) and (■) MC results at 298.15 and 288.15 K, respectively. (⊙) and (▲) Experimental measurements of Rolniak and Kobayashi for zeolite 13*X* at 298.15 and 288.15 K, respectively.

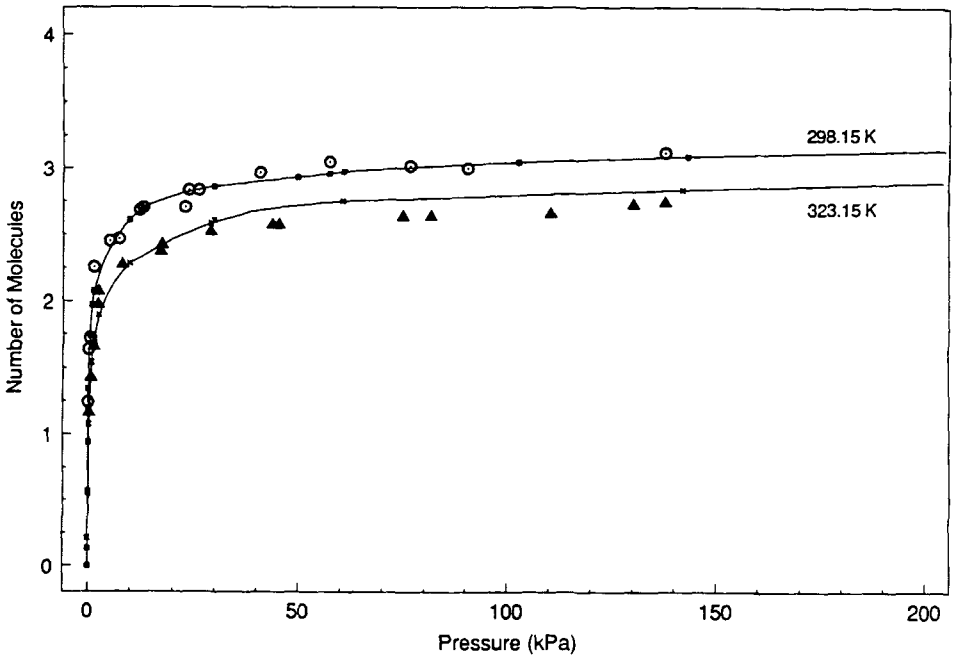

Figure 8 Average occupancy as a function of pressure for i-C_4H_{10} in a $13X$ cavity. (■) and (×) MC results at 298.15 and 288.15 K, respectively. (⊙) and (▲) Experimental measurements of Hyun and Danner for zeolite $13X$ at 298.15 and 288.15 K, respectively.

polarizability and relative positions of individual atoms of the molecule and agreement with experiment is usually within 5%. Equations (1) and (2) are used for the adsorbate–adsorbent interactions.

Figure 7 presents the isotherms of methane absorbed in zeolite $13X$ at 298.15 and 288.15 K. The GCMC isotherms are compared with the experimental measurements of Rolniak and Kobayashi [29]. The simulations agree with the experimental data within 5%. Because of its comparatively shallow Lennard–Jones potential well, CH_4 adsorbs weakly compared to xenon.

The GCMC isotherms of isobutane adsorbed in zeolite $13X$ at 298.15 and 323.15 K are compared with experimental measurements of Hyun and Danner [30] in Figure 8. The agreement between simulation and experiment is excellent up to a pressure of 50 kPa. At higher pressures there is a systematic deviation of about 10% between predicted and experimental data.

Table 3 gives the percentage contributions of fluid–fluid and fluid–solid interactions to the configurational energy of adsorption for methane and isobutane. Since the saturation capacity of the cavity for isobutane is only 4 molecules, its fluid–fluid interactions are less than 10% of the total energy.

Figure 9 presents the MC results calculated from Equations (14)–(15) for the isosteric heat of CH_4 absorbed in zeolite $13X$ at 298.15 K. The simulation results are compared with the experimental measurements of Chkhaidze *et al.* [31] for CH_4 adsorbed in NaX at 273.15 K. The GCMC data show an almost linear increase with coverage at low and medium occupancy due to the cooperative effect of fluid–fluid

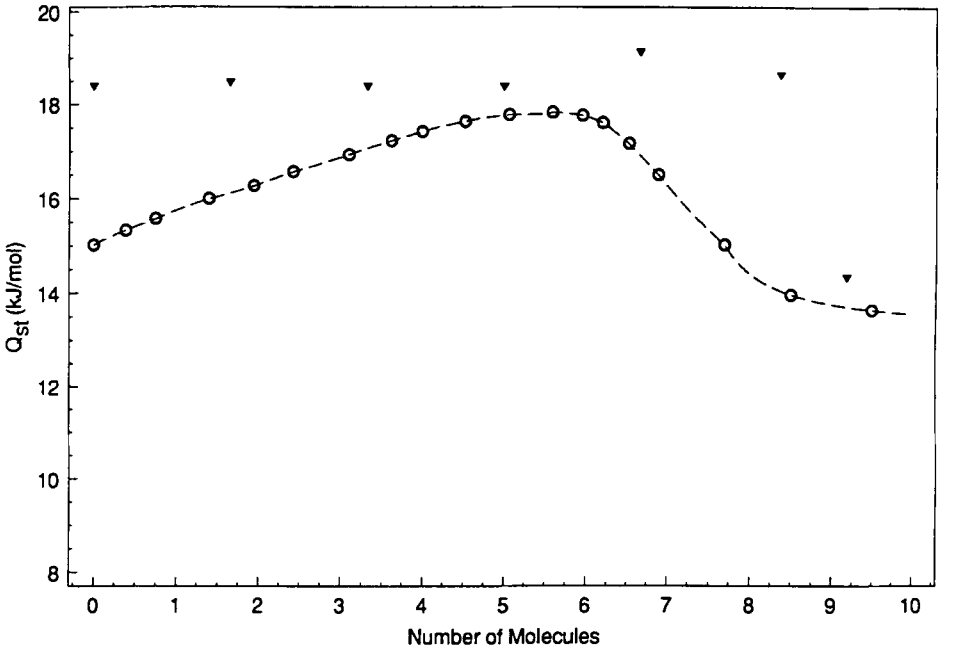

Figure 9 Isosteric heat as a function of coverage for CH_4 in zeolite 13*X*. (⊙) MC results at 298.15 K. (▼) Experimental measurements of Chkhaidze *et al.* at 210.9 K.

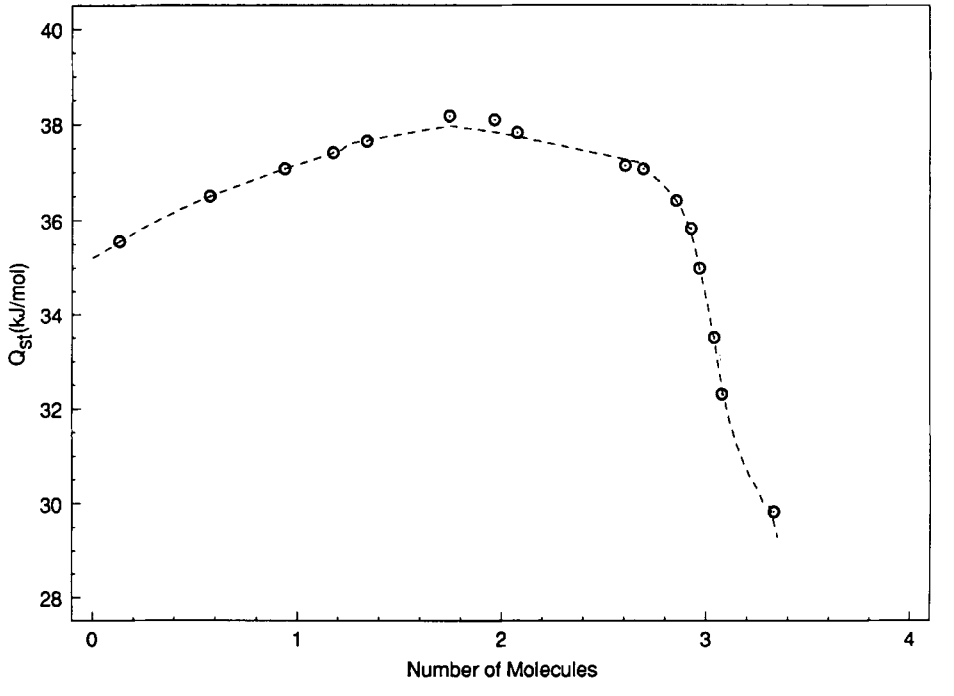

Figure 10 Isosteric heat as a function of coverage for *i*-C_4H_{10} in zeolite 13*X*. (⊙) MC results at 298.15 K.

interactions. The isosteric heat passes through a maximum at a coverage of 5 molecules per cavity and then drops because of the contribution of the bulk fluid term in equation (14) at high pressures. The experimental measurements also pass through a maximum, but the low and medium coverage experimental heat does not exhibit the linear increase of the GCMC results. The most likely explanation is that the 'sphericalization processes' applied to the dispersion adsorbate–adsorbate potential results in an almost energetically homogeneous surface in which the cooperative effect is more pronounced than in the real system.

The isosteric heat of isobutane at 298.15 K is presented in Figure 10. The data show the same linear increase with respect to coverage as CH_4. However at an average occupancy of 2 molecules per cavity, the isosteric heat shows a turndown which becomes sharp at a coverage of 3 molecules. As will be discussed later, the model cavity has four high energy adsorption sites. Because of their size, isobutane molecules cannot occupy all four sites simultaneously. When coverage increases beyond two molecules, less energetically favorable positions are occupied and the isosteric heat drops.

Density profiles of CH_4 in the zeolite cavity have been calculated at 298.15 K by analyzing the configurations collected from the MC simulations. Local density inside the cavity depends on three spatial coordinates (r, θ, ϕ). The average density with respect to the coordinates (θ, ϕ) (one body distribution function) is presented as a function of the radius r in Figure 11. Three density profiles have been plotted for low, medium and high coverage. The zero of the horizontal axis corresponds to the center of the cavity and the first layer of oxygen ions are located at 7 Å. At low and medium coverage there is a single peak at a distance of 3.5–4 Å from the center of the cavity; therefore all the centers of the adsorbed methane molecules are located in a spherical shell. As the saturation capacity is approached, one more peak appears at the center of the cavity. Although there is a significant localization of adsorption along the r

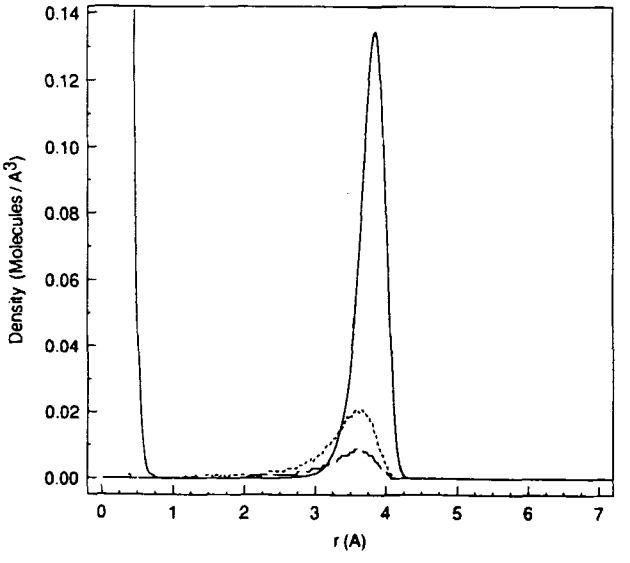

Figure 11 Density profiles as a function of the radius of a 13X cavity for CH_4. (--) $\langle N \rangle$ = 1.0; (---) $\langle N \rangle$ = 2.5; (—) $\langle N \rangle$ = 11.1.

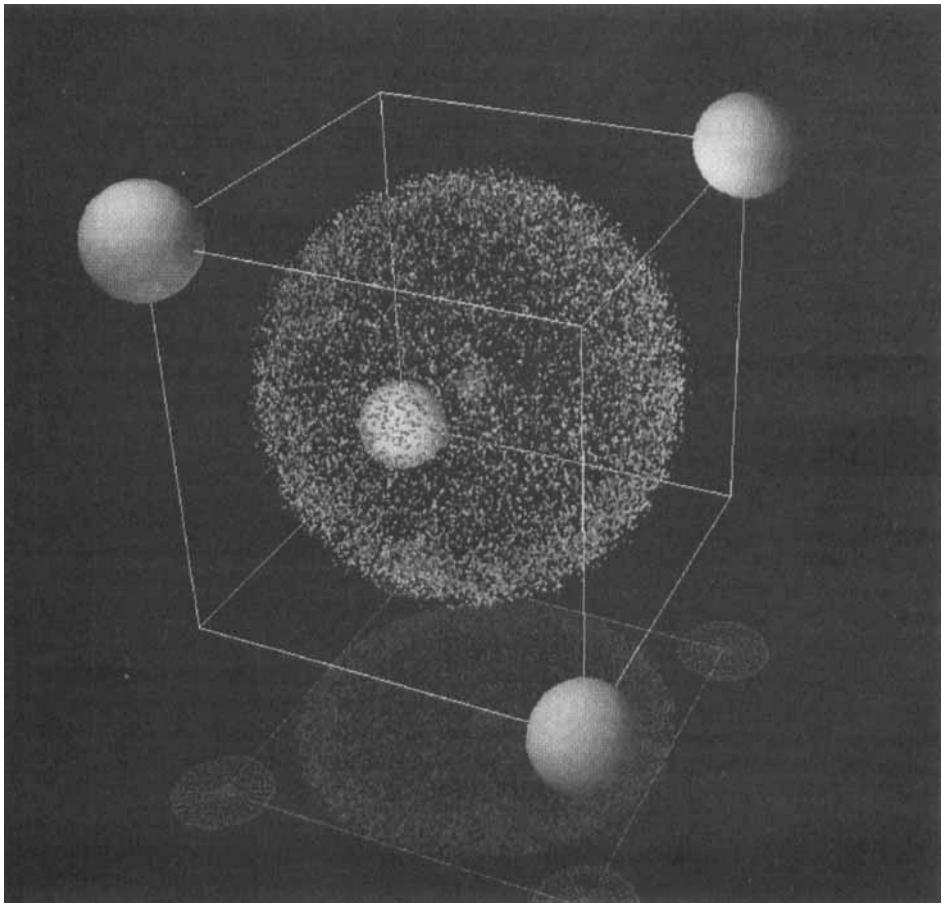

Figure 12 (*See* Color Plate I) Density and energy distribution of CH_4 in a zeolite cavity of type *X*. The four cations II are located at the edges of a cube 6.8 Å from the center of the cavity. Each spot inside the cube represents the position occupied by the center of mass of the adsorbed molecule at different MC steps. The color of the spot is a measure of the energy of the adsorbed molecule. The energy changes in the order: red (− 50 kJ/mol), yellow, green, cyan, blue (0 kJ/mol). ($\langle N \rangle = 10$.)

axis, methane molecules are distributed rather uniformly with respect to the (θ, ϕ) coordinates both at low and high coverage, Figure 12. Local density peaks at positions opposite the four cations II are about 50% higher than those for average density. At these sites the electric field attains its maximum value; since the induced electrostatic interactions are a function of the electric field, energy minima are found near the cations.

Isobutane shows a similar structure inside the zeolite. The molecules are located in a spherical shell at a distance of 3–3.5 Å from the center of the cavity, leaving the rest of the space void. Since no more than four molecules are present in a supercage, no additional peak near the center of the cavity is found even at saturation capacity. At

high coverage, the local density is 3–4 times larger than average at positions opposite the four cations II because of induced electrostatic interactions.

Adsorption of Lennard-Jones Molecules with Point Quadrupole Moments: Carbon Dioxide and Ethylene

Carbon dioxide is a linear molecule with a large quadrupole moment. Because of the axial symmetry of carbon dioxide its quadrupole moment tensor is fully defined by the Q_{zz} component. Carbon dioxide was modeled by a Lennard–Jones potential with a point quadrupole moment, Equations (7) and (10). Ethylene is a planar molecule with a quadrupole moment. Since ethylene has an axis of two-fold symmetry, the quadrupole tensor requires the specification of two independent components. The value listed for the quadrupole moment of ethylene in Table 2 is an effective scalar quadrupole moment determined by fitting experimental data of bulk-phase second virial coefficients. Interactions of carbon dioxide and ethylene with the zeolite crystal are described by equations (1)–(5).

The GCMC isotherms of carbon dioxide adsorbed in zeolite 13*X* at 298.15 and 323.15 K are compared with experimental measurements of Hyun and Danner [30] in Figure 13. Although the predicted and experimental isotherms cross each other twice, the average agreement between simulation and experiment is within 15% across the range of pressures for which experimental data are available. Carbon dioxide is much more strongly adsorbed than methane: at 100 kPa and 298.15 K, the CO_2 coverage is

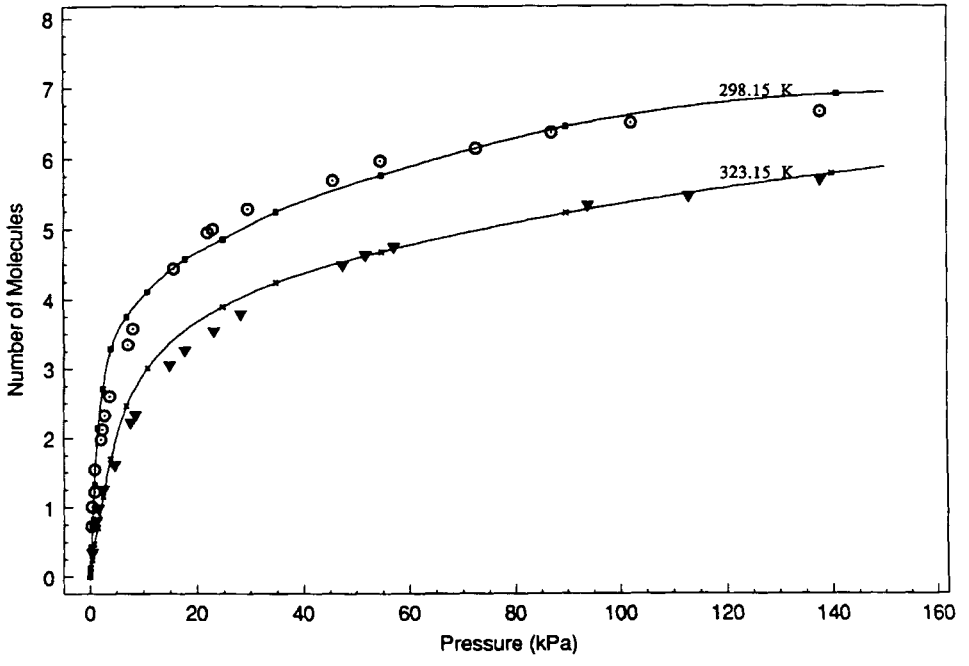

Figure 13 Average occupancy as a function of pressure for CO_2 in a 13*X* cavity. (■) and (×) MC results at 298.15 and 323.15 K, respectively. (⊙) and (▼) Experimental measurements of Hyun and Danner for zeolite 13*X* at 298.15 and 323.15 K, respectively.

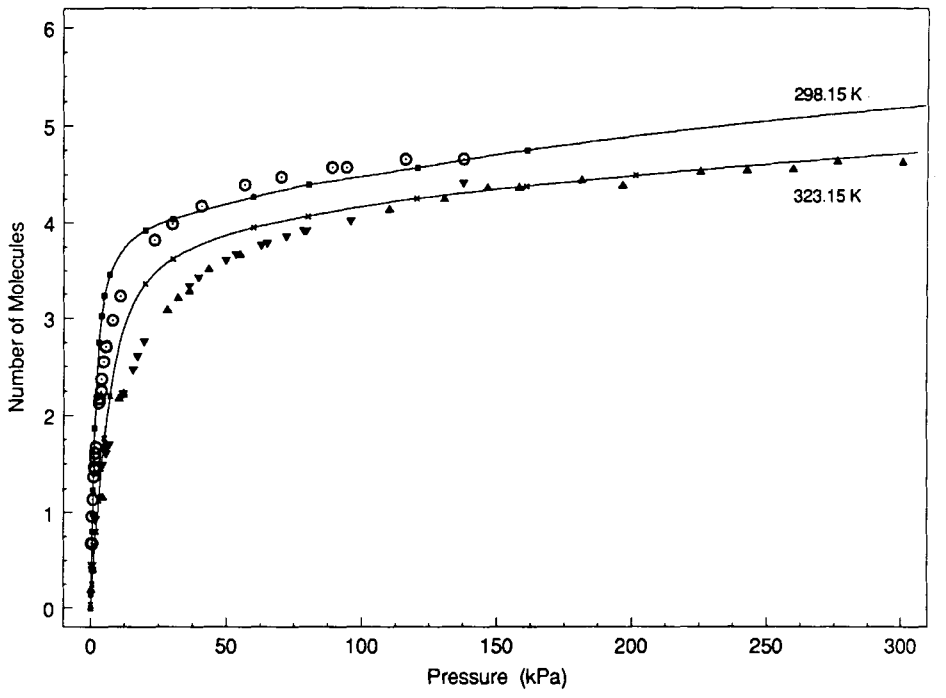

Figure 14 Average occupancy as a function of pressure for C_2H_4 in a 13*X* cavity. (■) and (×) MC results at 298.15 and 323.15 K, respectively. (⊙) and (▼) Experimental measurements of Hyun and Danner for zeolite 13*X* at 298.15 and 323.15 K, respectively. (▲) Experimental measurements of Kaul for zeolite 13*X* at 323.15 K.

6 molecules per cavity and CH_4 is less than 0.5. As will be shown, the interaction of carbon dioxide's quadrupole moment with the electric field generated by the zeolite ions is mainly responsible for the higher adsorptivity of CO_2 in faujasite. In activated carbon where electrostatic interactions are less important, the difference in the strength of adsorption of CH_4 and CO_2 is smaller [32].

Figure 14 presents our results for the isotherms of ethylene at 298.15 and 323.15 K. The GCMC isotherms are compared with experimental measurements of Hyun and Danner [30] for ethylene adsorbed in zeolite 13*X* at 298.15 and 323.15 K and those of Kaul [33] at 323.15 K. Agreement between simulation and experiment is not as good as for CO_2. Although MC results are close to experimental data at low and high coverage, there is a systematic deviation of about 25% at moderate pressures. The most likely explanation for this discrepancy is that the point quadrupole approximation is less successful for molecules whose quadrupole tensor is described by more than one component. For such molecules, an alternative is to assign charges to each individual atom of the molecule and let them interact through a coulombic potential with the zeolite cations. However such a model increases the required simulation time dramatically.

Less ethylene than carbon dioxide is absorbed at saturation. Ethylene has a larger collision diameter than CO_2 (see Table 2) and therefore its saturation capacity is about 9 molecules per cavity, compared to 13 for CO_2 and CH_4.

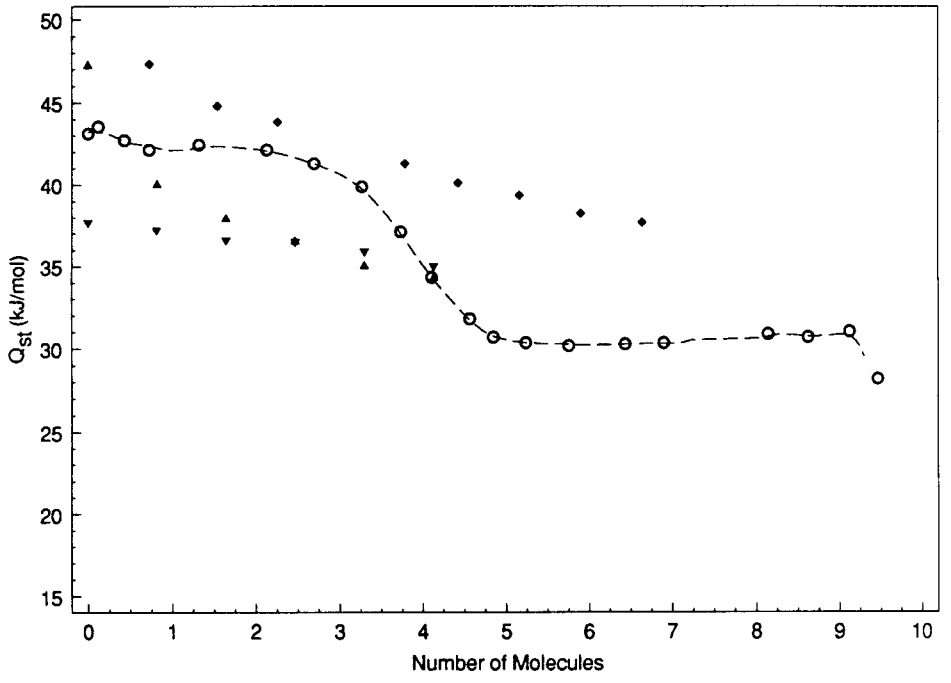

Figure 15 Isosteric heat as a function of coverage for CO_2 in zeolite 13*X*. (⊙) MC results at 298.15 K. (▲, ▼) Data from differentiation of experimental isotherms of Hyun and Danner for CO_2 in zeolite 13*X*. (◆) Data from differentiation of experimental isotherms of Barrer and Gibbons for CO_2 in zeolite Na*X*.

For carbon dioxide and ethylene, Table 3 shows that the ion–quadrupole interaction contributes almost as much as dispersion to the energy of adsorption. Since the electrostatic energy is a strong function of the spatial coordinates, the zeolite cavity provides an energetically heterogeneous surface for the adsorption of molecules with large multipolar moments.

The isosteric heat of carbon dioxide at 298.15 K calculated from equations (14)–(15) is presented in Figure 15. The MC results are compared with data obtained from differentiation with respect to temperature of experimental isotherms of Hyun and Danner [17,30] and Barrer and Gibbons [34]. Our results fall mid-way between the two sets of experimental data. At low coverage, the isosteric heat drops slightly with average occupancy. However at a coverage of 3–5 molecules per cavity there is a sharp drop from 42 to 30 kJ/mole. The model used in these simulations has four major adsorption sites in each supercage located at positions close to the four cations II (Table 1). The sharp drop corresponds to saturation of the energy minima and generation of configurations with molecules at less favorable positions. At medium to high coverage, the isosteric heat of carbon dioxide is constant up to the saturation capacity, where it drops because of the contribution of bulk fluid terms at high pressures.

The isosteric heat of C_2H_4 is presented in Figure 16 at 298.15 K. It exhibits behavior

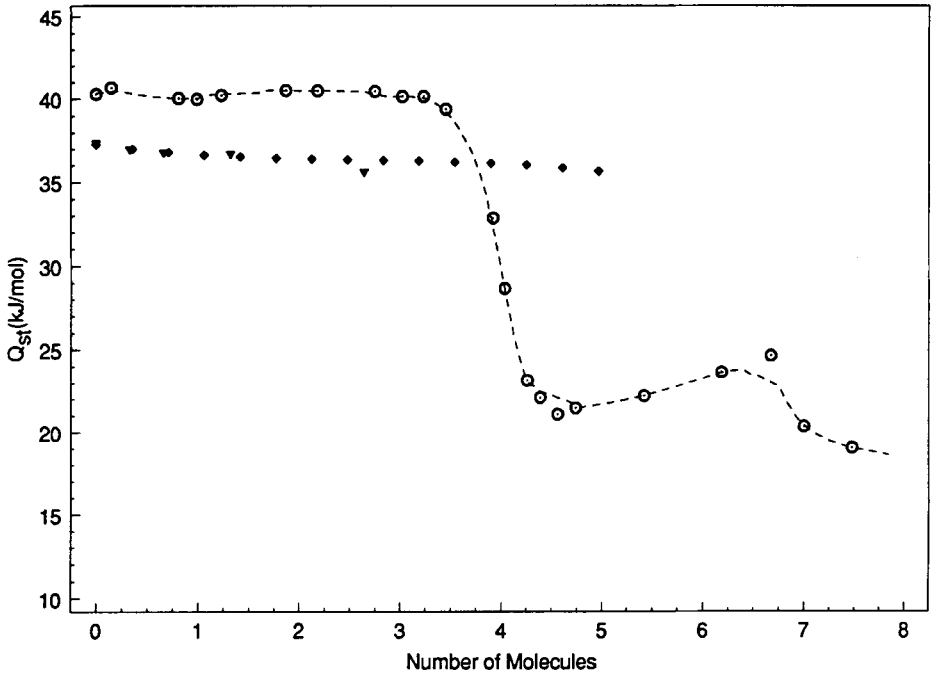

Figure 16 Isosteric heat as a function of coverage for C_2H_4 in zeolite 13*X*. (⊙) MC results at 298.15 K. (▼) Data from differentiation of experimental isotherms of Hyun and Danner for C_2H_4 in zeolite 13*X*. (◆) Data from differentiation of experimental isotherms of Bezus *et al.* for C_2H_4 in zeolite Na*X*.

results with data obtained by differentiation of experimental isotherms of Hyun and Danner [17,30] and Bezus *et al.* [35] shows that at low and moderate coverage MC simulation overestimates the isosteric heat by about 10%. The isosteric heat curves of CO_2 and C_2H_4 in zeolite 13*X* show a rich structure because of the energetic heterogeneity of the surface.

Density profiles are presented in Figure 17, for three different occupancies: low, medium and high. Figure 17a presents the average density with respect to (θ, ϕ) coordinates as a function of the third coordinate r. To demonstrate the high concentration of CO_2 molecules at certain sites, the local density along solid angles of 0.04 steradians facing the four cations II is plotted in Figure 17b. These particular orientations correspond to energy minima located opposite the cations. At low and medium coverage, there is a single peak between 3 and 4 Å from the center; all molecular centers are located inside this spherical shell. At high coverage close to the saturation capacity, one more peak appears near the center of the cavity.

The localization effect can be seen by comparing Figure 17a and 17b. The density peaks which appear along the axis that connect the center with the cations II are more than 10 times higher than those of the average density profiles. The electric field is a maximum at positions close to the sodium cations II and its interaction with the quadrupole moment of carbon dioxide generates energy minima much deeper than in the case of methane adsorption. This results in highly localized adsorption for CO_2 at low and medium coverage.

The spatial and energy distribution of the adsorbed molecules is demonstrated in

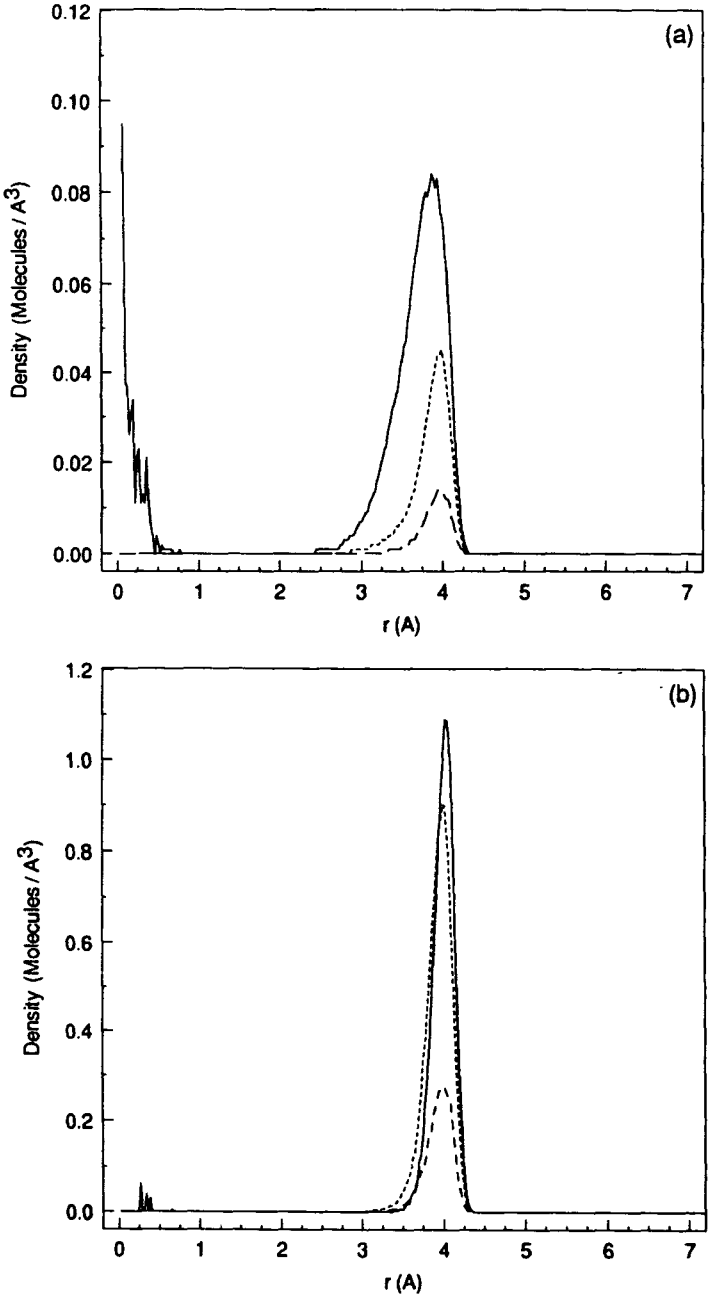

Figure 17 Density profiles as a function of the radius of a 13*X* cavity for CO_2. (--) $\langle N \rangle = 1.0$; (---) $\langle N \rangle = 3.7$; (—) $\langle N \rangle = 9.8$ (a) Average density (θ, ϕ) (b) Local density at positions of energy minima.

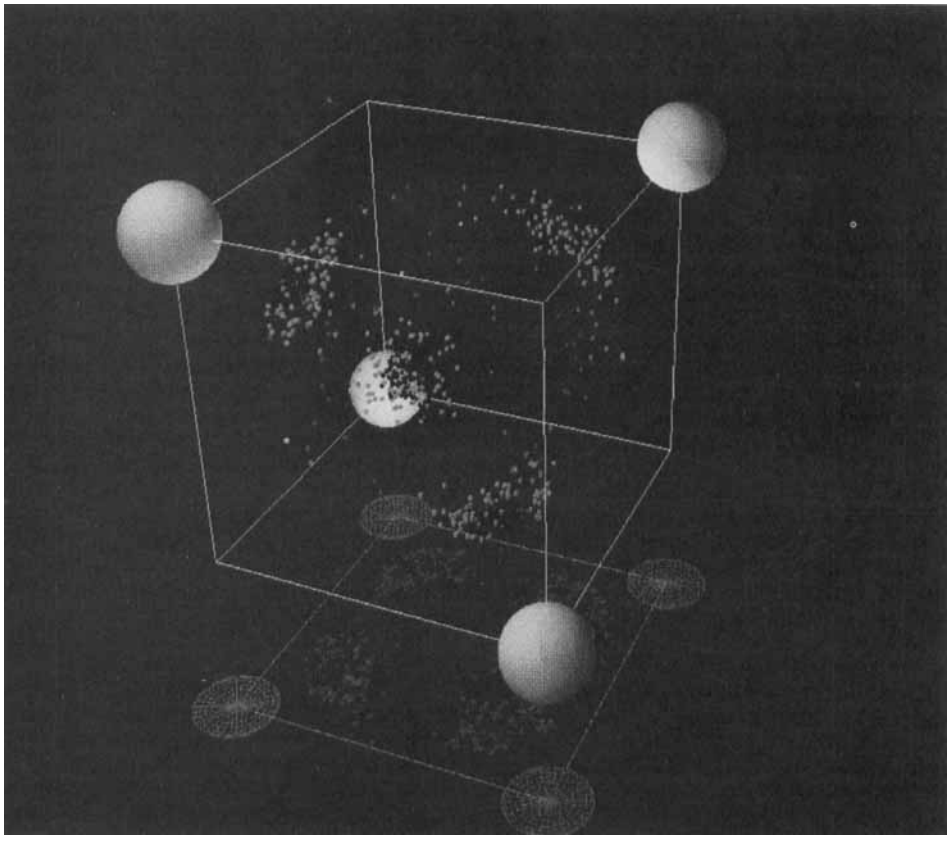

Figure 18a (*See* Color Plate II) Density and energy distribution of CO_2 in a zeolite cavity of type *X*. The four cations II are located at the edges of a cube 6.8 Å from the center of the cavity. Each spot inside the cube represents the position occupied by the center of mass of the adsorbed molecule at different MC steps. The color of the spot is a measure of the energy of the adsorbed molecule. The energy changes in the order: red(− 50 kJ/mol), yellow, green, cyan, blue (0 kJ/mol). $\langle N \rangle = 1$.

similar to CO_2, with a constant value of isosteric heat (40 kJ/mol) up to a coverage of 4 molecules per cavity. The sharp drop in the heat occurs at an average occupancy of 4 molecules because of saturation of the four energy minima. Comparison of our during 1,000 MC steps randomly selected are presented in Figure 12 and 18, respectively. The four sodiums II are located at the edges of a cube at a distance of 6.8 Å from the center of the cavity. Methane is uniformly distributed but carbon dioxide is the 3-D diagrams; the positions occupied by methane and carbon dioxide molecules during 1,000 MC steps randomly selected are presented in Figure 12 and 18, respectively. The four sodiums II are located at the edges of a cube at a distance of 6.8 Å from the center of the cavity. Methane is uniformly distributed but carbon dioxide is highly localized close to the cations II because of the attractive interactions discussed before. A comparison of Figure 18a and 18b shows that as the coverage increases, CO_2 molecules occupy less energetically favorable positions; this causes the isosteric heat

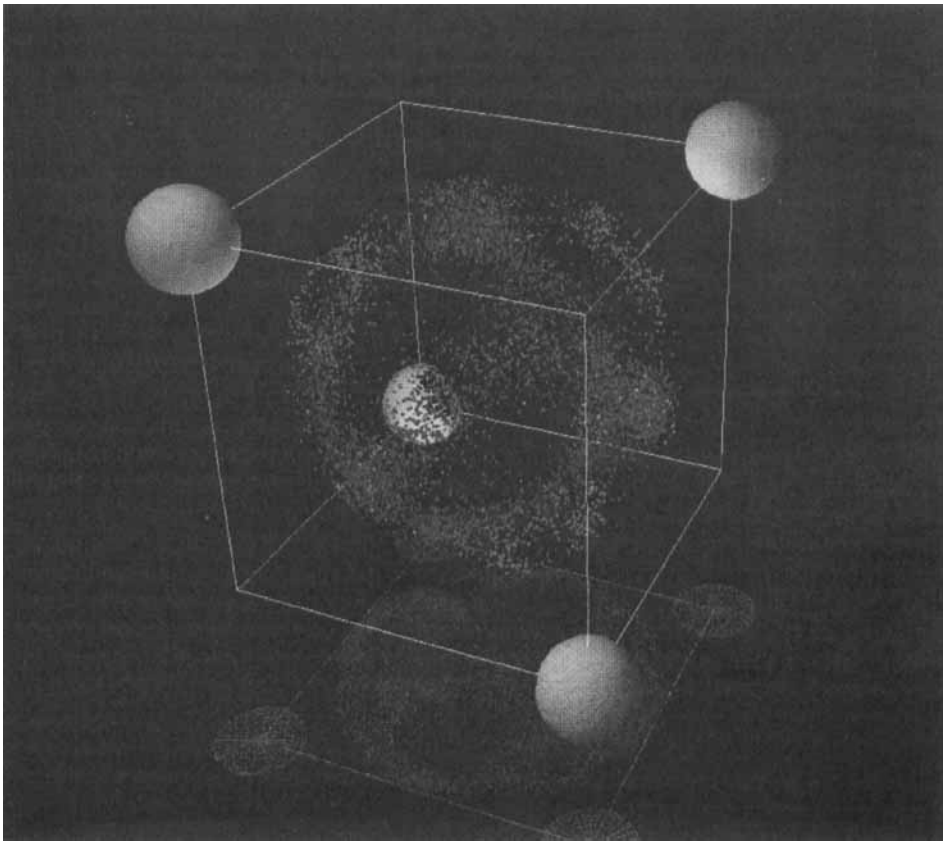

Figure 18b (*continued*) (*See* Color Plate III) ($\langle N \rangle$ = 10.)

to drop. For methane the cavity is rather homogeneous energetically, since all the sites occupied by methane have similar energies, Figure 12.

Ethylene has a smaller quadrupole moment than CO_2; it shown the same structure as CO_2, although the localization effect close to the cations II is less pronounced. However, only one peak at 4 Å from the center of the cavity appears in its density distribution, even at high coverage close to saturation. Because of its size, ethylene cannot fit in the center of the cavity when the four high-energy sites are filled.

In summary, the zeolite cavity is either a homogeneous surface or a highly heterogeneous one, depending on the molecular characteristics of the adsorbed gas and the type, position and charge of the zeolite cations. For highly polar molecules, the electric field inside the zeolite crystal has to be incorporated in the model because its interaction with multipolar moments accounts for a significant fraction of the total energy.

As mentioned before the potential energy has two adjustable parameters, ($C\,\varepsilon_{is}$) and σ_{is}, which are obtained by fitting adsorption second virial coefficients versus temperature to experimental data. The two adjustable parameters should comply

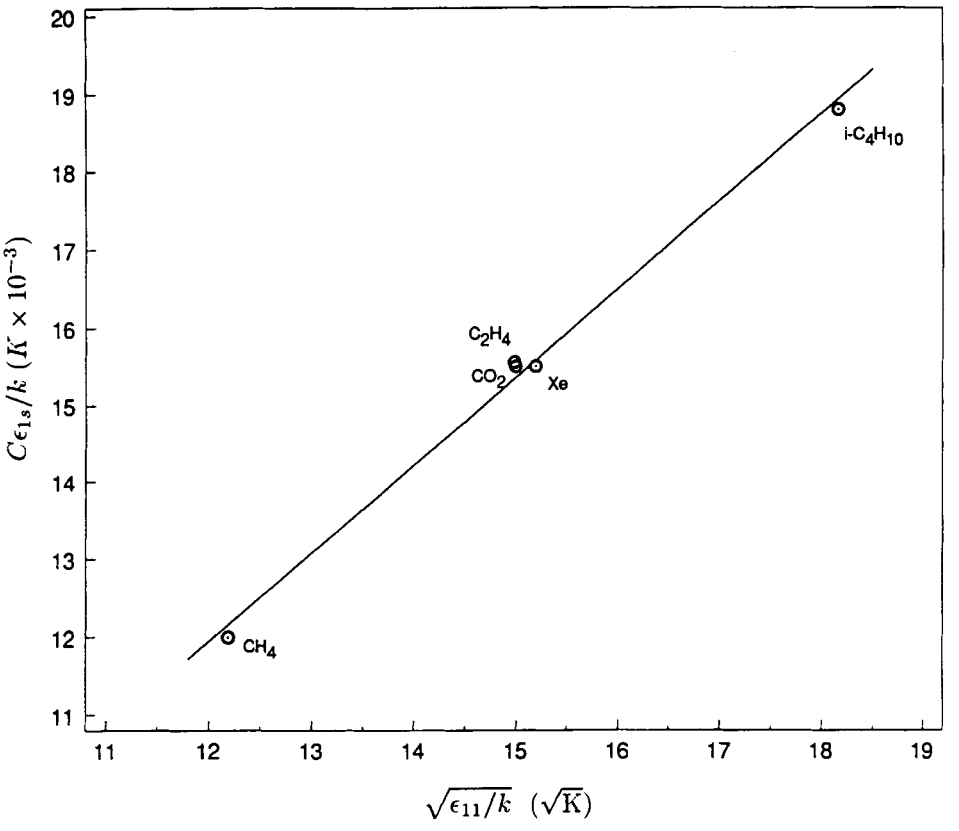

Figure 19 Well depth of the LJD potential versus the LJ depth of the adsorbed molecule.

approximately with the following mixing rules:

$$\sigma_{is} = \frac{1}{2}(\sigma_{ii} + \sigma_{ss}) \tag{18}$$

$$C\varepsilon_{is} = C\sqrt{\varepsilon_{ii}\varepsilon_{ss}}$$

where ε_{ss} and σ_{ss} are the effective Lennard–Jones parameters of the zeolite crystal ions and ε_{ii} and σ_{ii} are the potential depth and collision diameter of the adsorbed molecule. During the fitting procedure the parameters ($C\varepsilon_{is}$) and σ_{is} were selected so that their deviation from Equation (18) is within 1% and 3%, respectively. In Figures 19 and 20, ($C\varepsilon_{is}$) and σ_{is} are plotted versus $\sqrt{\varepsilon_{ii}}$ and σ_{ii}, respectively, for the five components involved in these simulations. In the collision diameter diagram, Figure 20, the deviation between the values used in these simulations and a straight line of slope 0.5 is within 3% except for i-C_4H_{10} which is within 5%.

CONCLUSIONS

Grand canonical Monte Carlo simulations have been performed for single-gas

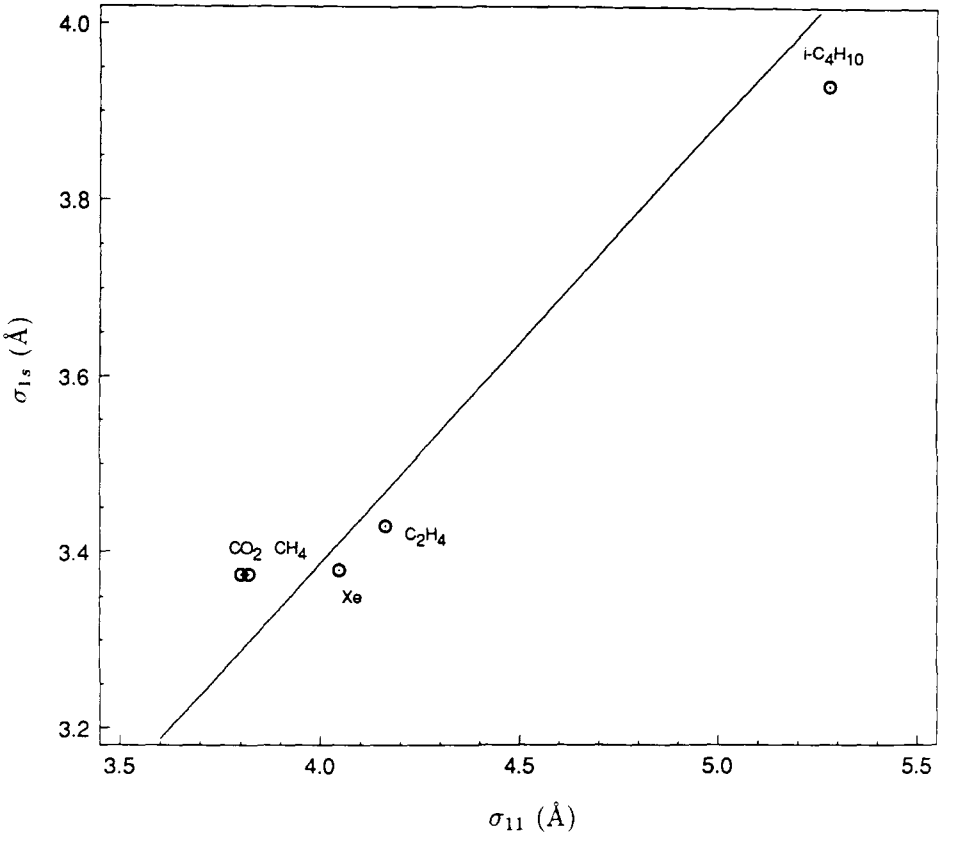

Figure 20 Collision diameter of the LJD potential versus the LJ diameter of the adsorbed molecule.

adsorption of Lennard–Jones molecules with point multipole moments in zeolite cavities of type *X*. A spherically-averaged potential was adopted for the dispersion and repulsion interaction of adsorbate molecules with the adsorbent. The induced electrostatic potential and the interactions of the point multipole moments with the electric field generated by the zeolite cations were taken into account. Thermodynamic and structural properties have been calculated for Xe, CH_4, CO_2, C_2H_4, and i-C_4H_{10}.

Quantitative agreement between the simulation and experimental measurements was achieved by fitting the parameters $C\varepsilon_{is}$ and σ_{is} of the Lennard–Jones Devonshire potential to experimental data of adsorption second-virial coefficients. The ability of the simulation to predict the adsorption isotherm at different temperatures indicates that the proposed model is satisfactory for spherical and linear molecules with multipole moments.

Isosteric heats were calculated from ensemble fluctuations. Internal consistency of the simulations was tested by comparing the integral of the differential heat obtained by the fluctuation method with the total energy, which is an ensemble average. The contribution of individual potentials to the total energy of adsorption was evaluated. Adsorbate–adsorbate interactions constitute up to 20% of the energy of adsorption

in molecular sieves. Interactions between molecules adsorbed in different cavities make a significant contribution to the total energy of adsorption. The quadrupole moment of CO_2 is mainly responsible for its high adsorptivity.

Density profiles of the adsorbed molecules were calculated. The distributions of the adsorbed fluid indicate that the zeolite cavity is a homogeneous surface or a highly heterogeneous one, depending on the molecular characteristics of the adsorbed gas and the type, position, and charge of the zeolite cations.

In summary, the work presented here shows that MC simulations can be used for predicting adsorption equilibrium in molecular sieves. Furthermore, they generate consistent data that can be used for testing thermodynamic and statistical theories for single-gas and multicomponent adsorption.

Acknowledgements

We thank Dr. N.I. Badler and Welton Becket of the Computer Graphics Research Laboratory, University of Pennsylvania for their help on preparing our color graphics. Support by the Gas Research Institute Contract #5084-260-1254 and by National Science Foundation grant 88-10215 is gratefully acknowledged.

References

[1] H.J.F. Stroud, E. Richards, P. Limcharoen and N.G. Parsonage, "Thermodynamic study of the Linde sieve 5A + Methane system", *J. Chem. Soc., Faraday Trans. 1*, **72**, 942 (1976).

[2] T.L. Hill, *An Introduction to Statistical Thermodynamics*, Dover (1986), p. 290.

[3] J.L. Soto and A.L. Myers, "Monte Carlo studies of adsorption in molecular sieves", *Mol. Phys.*, **42**, 971 (1981).

[4] A.G. Bezus, A.V. Kiselev, A.A. Lopatkin and Pham Quang Du, "Molecular statistical calculation of the thermodynamic adsorption characteristics of zeolites using the atom–atom approximation. Part 1.-Adsorption of methane by zeolite Na*X*", *J. Chem. Soc., Faraday Trans. 2*, **74**, 367 (1978).

[5] A.V. Kiselev and Pham Quang Du, "Molecular statistical calculation of the thermodynamic adsorption characteristics of zeolites using the atom–atom approximation. Part 2.-Adsorption of non-polar and polar inorganic molecules by zeolites of type *X* and *Y*", *J. Chem. Soc., Faraday Trans. 2*, **77**, 1 (1981).

[6] A.V. Kiselev and Pham Quang Du, "Molecular statistical calculation of the thermodynamic adsorption characteristics of zeolites using the atom–atom approximation. Part 3.-Adsorption of hydrocarbons", *J. Chem. Soc., Faraday Trans. 2*, **77**, 17 (1981).

[7] R.L. June, A.T. Bell, D.N. Theodorou, "Prediction of sorption and diffusion in zeolite catalysts", *J. Phys. Chem.*, **94**, 1508 (1990).

[8] G.B. Woods, A.Z. Panagiotopoulos and J.S. Rowlinson, "Adsorption of fluids in model zeolite cavities", *Mol. Phys.*, **63**, 49 (1988).

[9] G.B. Woods and J.S. Rowlinson, "Computer simulations of fluids in zeolite *X* and *Y*", *J. Chem. Soc., Faraday Trans. 2*, **85**(6), 765 (1989).

[10] D.M. Razmus and C.K. Hall, "Prediction of the adsorption of gases in 5A zeolites using Monte Carlo simulation", AIChE Annual Meeting, San Fransisco, CA (1989).

[11] S. Yashonath, J.M. Thomas, A.K. Nowak and A.K. Cheetham, "The siting, energetics and mobility of saturated hydrocarbons inside zeolitic cages: methane in zeolite *Y*", *Nature*, **331**, 601 (1988).

[12] S. Yashonath, P. Demontis and M.L. Klein, "A molecular dynamics study of methane in zeolite Na*Y*", *Chem. Phys. Letters*, **153**, 551 (1988).

[13] J.L. Soto, P.W. Fisher, A.J. Glessner and A.L. Myers, "Sorption of gases in molecular sieves", *J. Chem. Soc., Faraday Trans. 1*, **77**, 157 (1981).

[14] L. Broussard and D.P. Shoemaker, "The structures of synthetic molecular sieves", *J. Am. Chem. Soc.*, **82**, 1041 (1960).

[15] A.D. Buckingham, "Permanent and induced molecular moments and long-ranged intermolecular forces", *Adv. Chem. Phys.*, vol. 12, 107, John Wiley, New York (1967).

[16] G. Ravilatera, J.C. Carru and A. Chapoton, "Interpretation of the "Intermediate Frequency" Di-electric Spectra of Synthetic Zeolites *X*", *J. Chem. Soc., Faraday Trans. 1*, **73**, 843 (1977).
[17] D.P. Valenzuela and A.L. Myers, *Adsorption Equilibrium Data Handbook*, Prentice Hall, New Jersey (1989).
[18] K.E. Gubbins and C.H. Twu, "Thermodynamics of polyatomic fluid mixtures-I", *Chem. Eng. Science*, **33**, 863 (1978).
[19] M.P. Allen and D.J. Tildesley, *Computer Simulation of Liquids*, Oxford University Press, New York (1987).
[20] D.J. Adams, "Calculating the low temperature vapour line by Monte Carlo", *Mol. Phys.*, **29**, 307 (1975).
[21] B.K. Peterson and K.E. Gubbins, "Phase transitions in a cylindrical pore. Grand canonical Monte Carlo, mean field theory and the Kelvin equation", *Mol. Phys.*, **62**, 215 (1987).
[22] J.A. Barker and D. Henderson, "What is "liquid"? Understanding the States of Matter", *Rev. Mod. Phys.*, **48**, 587 (1976).
[23] M. Mezei, "Grand-canonical Ensemble Monte Carlo Study of Dense Liquid Lennard-Jones, Soft Spheres and Water", *Mol Phys.*, **61**, 565 (1987).
[24] R.C. Reid, J.M. Prausnitz and T.K. Sherwood, *The Properties of Gases and Liquids*, McGraw-Hill Book Company, New York (1977).
[25] D. Nicholson and N.G. Parsonage, *Computer Simulation and the Statistical Mechanics of Adsorption*, Academic Press, New York (1982).
[26] B.G. Aristov, V. Bosachek and A.V. Kiselev, "Adsorption of Xenon by Li*X* and Na*X* zeolite crystals", *Colloid J. USSR*, **29**, 557 (1967).
[27] A.A. Fomkin, V.V. Serpinskii and B.P. Bering, *Bull. Acad. Sci., USSR, Div. Chem. Sci.*, **24**, 1813 (1975).
[28] J. Applequist, J.R. Carl and K. Fung, "An atom dipole interaction for molecular polarizability. Application to polyatomic molecules and determination of atom polarizabilities.", *J. Am. Chem. Soc.*, **94**, 2950 (1972).
[29] P.D. Rolniak and R. Kobayashi, "Adsorption of methane and several mixtures of methane and carbon dioxide at elevated pressures and near ambient temperatures on 5A and 13*X* molecular sieves by tracer perturbation chromatography", *AIChE J.*, **26**, 616 (1980).
[30] S.H. Hyun and R.P. Danner, "Equilibrium adsorption of ethane, ethylene, isobutane, carbon dioxide, and their binary mixtures on 13X molecular sieves", *J. Chem. Eng. Data.*, **27**, 196 (1982).
[31] E.V. Chkhaidze, A.A. Fomkin, V.V. Serpinskii and G.V. Tsitsishvilli, "Application of the theory of volume filling of micropores to methane adsorption on a microporous carbonaceous adsorbent", *Izv. Akad. Nauk USSR, Ser. Khim.*, 276 (1989).
[32] L. Szepesy and V. Illes, "Adsorption of gases and gas mixtures", *Acta Chim. Hung.*, **35**, 37 (1963).
[33] B.K. Kaul, "Modern version of volumetric apparatus for measuring gas-solid equilibrium data", *Ind. Chem. Res.*, **26**, 928 (1987).
[34] R.M. Barrer and R.M. Gibbons, "Zeolite carbon dioxide: energetics and equilibria in relation to exchangeable cations in faujasite", *Trans. Faraday Soc.*, **61**, 948 (1965).
[35] A.G. Bezus, A.V. Kiselev, Z. Sedlacek and Pham Quang Du, "Adsorption of ethane and ethylene on *X*-zeolites containing Li, Na, K. Rb and Cs cations", *Trans. Faraday Soc.*, **67**, 468 (1971).
[36] W.A. Steele, *The Interaction of Gases with Solid Surfaces*, Pergamon Press, Oxford (1974).
[37] A.Z. Panagiotopoulos, U.W. Suter and R.C. Reid, "Phase diagrams of nonideal fluid mixtures from Monte Carlo simulation", *Ind. Eng. Chem. Fund.*, **25**, 525 (1986).
[38] J.O. Hirschfelder, C.F. Curtiss and R.B. Bird, *Molecular Theory of Gas and Liquids*, Wiley, New York (1954).
[39] D.E. Strogryn and A.P. Strogryn, "Molecular multipole moments", *Mol. Phys.*, **11**, 371 (1966).